Sensors & Transducers, Vol. 237, Issue 9-10, September-October 2019, pp. 30-36

Sensors & Transducers

Published by IFSA Publishing, S. L., 2019
http://www.sensorsportal.com

Piezoelectric Ceramic Transducers as Time-Varying Displacement Sensors in Nanopositioners

[3] Massoud HEMMASIAN ETTEFAGH, [2] Mokrane BOUDAUD, [1, 2, *] Ali BAZAEI, [1] Zhiyong CHEN and [2] Stéphane RÉGNIER

[1] University of Newcastle, School of Electrical Engineering and Computing, Callaghan, NSW 2308, Australia
[2] Sorbonne University, Institute for Intelligent Systems and Robotics (ISIR), Paris, France
[3] Huazhong University of Science and Technology, School of Artificial Intelligence and Automation, Wuhan, China
[1] Tel.: +61 240238982, fax: +61 249216993
E-mail: Ali.Bazaei@newcastle.edu.au

Received: 30 August 2019 /Accepted: 27 September 2019 /Published: 30 November 2019

Abstract: We present a direct measurement of stage displacement in piezo-driven nanopositioners via piezoelectric (PZT) ceramics. In addition to compactness and affordability, our study shows that within the sensing bandwidth, the sensor is able to track time-varying large signal profiles of stage displacement accurately without utilizing signal conditioning devices. Also, the sensor can be used to capture cross coupling effect in orthogonal axes of motion. For the full-scale range, accuracy of the suggested sensor is less than 27 nm in the sensing bandwidths when the sensor is calibrated with a constant scaling factor. The 3σ-resolution of the sensor is 1.9 nm.

Keywords: Displacement sensor, Piezoelectric sensor, Nanopositioning stage, Time-varying displacement, Scanning.

1. Introduction

The accurate measurement of high frequency movement is essential for many micro and nano positioning systems including scanners in selective laser sintering applications [15-17], microscanner mirrors [12-14], and nanopostioners for scanning probe microscopy [1-11].

PZT sensors have many desired characteristics such as high bandwidth, small foot print, small noise level, compactness, and affordability [18]. The electromechanical coupling between electrical field and stress makes piezoelectric ceramics an ideal choice for strain, force, pressure, acceleration, and temperature measurement, and for energy harvesting [19-20]. Nevertheless, no study has been reported on piezoelectric ceramics to address the direct measurement of stage displacement in nanoposi-tioning systems, primarily because the sensor response exhibits drift and decreasing sensitivity at low frequencies from its RC high-pass characteristic. In scanning tasks, however, the high-pass decrease issue would not pose a problem since the displacement oscillates rapidly. In order to measure the displacement of nanopositioning stage directly, our study addresses the large signal characterization of piezoelectric ceramic response in a custom-made high-bandwidth Nanopositioner.

Few works employed piezoelectric ceramics as sensors in nanopositioners. In order to damp the dynamical vibration of a nanopositioners, the authors

in [8-9] employed stress induced voltage in piezo ceramics, without mentioning of or characterizing for direct displacement measurement. An application of piezoelectric materials in displacement measurement is reported in [21] in which the authors used piezo patches as a sensor-actuator pair. This work, however, needs bulky additional mechanical components that affects the displacement sensing bandwidth negatively.

In the present manuscript, we use a commercial PZT chip as a direct displacement sensor in a nanopositioning stage. In this respect, the performance of the PZT chip as a displacement sensor is characterized and analyzed. It is shown that the proposed sensor can measure stage displacement and cross coupling in a compact size parallel-structured nanopositiong stage with 3σ-resolution of 1.9 $[nm]$. In comparison with the authors' previous work in [22] and [23], this article characterizes the sensing performance of the PZT chip in measurement of cross coupling displacement between the horizontal axes of the nanopositioner. We also present a comprehensive study of the frequency responses of the proposed sensor and the stage displacement. In addition, we carry out identification procedures to approximate the responses by stable low-order linear models, which are suitable for feedback control design purposes. Some figures and tables are repeated here for convenience.

The rest of the paper is organized as follows. Section 2 presents the nanopositioning stage that is used in this study. In Section 3, experiment and frequency analysis of the PZT sensor are explained. In Section 4, we describe the characterization process of the PZT chip to be used as a direct displacement sensor. Section 5 analyzes the resolution of the proposed sensing method. We present the application of the PZT sensors in measurement of cross coupling displacement between the orthogonal horizontal axes in Section 6. Conclusions are given in Section 7.

2. Piezo-driven Compact Size Nanopositioning Stage with Embedded Piezo Ceramic Sensor

A schematic illustration of the piezo-driven x-y nanopositioning stage is shown in Fig. 1. In order to measure stage displacement along each horizontal axis, we installed a PZT chip in the axial direction of the PZT actuator. To prevent any induced parasitic voltage from PZT actuator to the displacement sensor, we have used an inactive ceramic insulator to separate the PZT sensor from the actuator. The main specifications of the piezo chip sensor and the PZT actuator are given in Table 1. We used the laser interferometric vibrometer described in [24] to calibrate the PZT sensor for measurement of stage displacement. In this respect, as shown in the inset of Fig. 1, the middle stage of the Nanopositioner is extruded 2 mm to provide a reflecting surface for the Laser beam. For each axis, the input voltage is amplified by an FLC Electronics A400DI voltage amplifier with a gain of 20 before being applied to the PZT stack actuator. In order to maximize the displacement of the middle stage, we fined-tuned the preload screws empirically. More details on the installation of the ceramic parts are reported in [22].

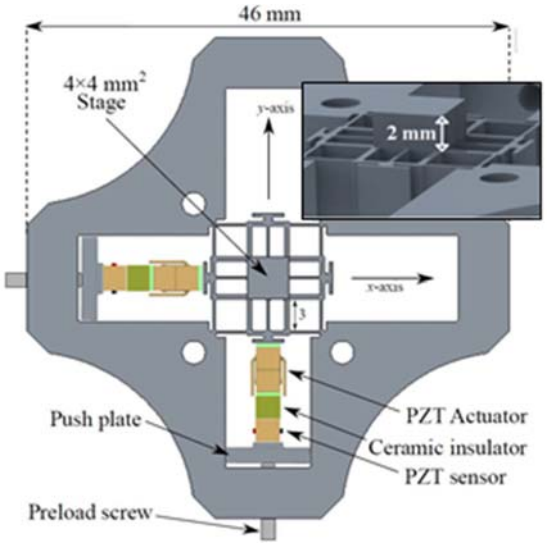

Fig. 1. Schematic illustration of the nanopositioning stage.

Table 1. Main specifications of sensor chip and actuator.

Physical Property, (V)	PZT Stack	PZT Chip
Drive Voltage Range	0-150 V	0-150 V
Free Stroke at 150 V	5.2 μm±15 %	2.3 μm±15 %
Recommended Preload	100 N	100 N
Blocking Force at 150 V	250 N	250 N
Dimensions in mm	2.5×2.5×5.0	2.5×2.5×2.3
Electric Capacitance	100 nF±15 %	50 nF±15 %
Resonance Frequency	250 kHz	650 kHz
Operating Temperature	−25-130°C	−25-130°C
Curie Temperature	230 °C	230 °C

3. Frequency Response of the Stage

Fig. 2 shows the frequency responses of the y-axis stage displacement from the Laser vibrometer and the y-axis PZT sensor voltage, respectively, with respect to the pre-amplified voltage applied to the y-axis actuator (y-axis input signal). Mathematical description of a piezo-driven Nanopositioner can be modeled accurately by a simple mass-spring damper model when the actuation frequency is below the first natural frequency [25]. Therefore, according to the collected data, the identified model of the Nanopositioning stage based on the laser vibrometer response of y-axis is

$$G_L = \frac{5.074 \times 10^9}{s^2 + 4793\, s + 1.16 \times 10^{10}} \qquad (1)$$

According to Fig. 2 and Eq. (1), the stage has a dominant resonance mode at 17.1 [kHz], its 3-dB bandwidth is 9.4 [kHz], and the damping ratio is $\zeta = 0.022$.

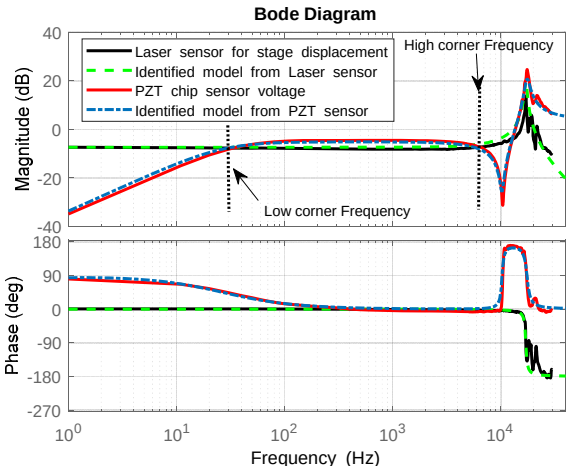

Fig. 2. Frequency response of y-axis.

Similarly, the identified model from the collected frequency response data of the PZT sensor voltage is

$$G_{PZT} = \frac{1.6\,(s+0.4)(s^2+3090\,s+4.13\times10^9)}{(s+167)(s^2+5706\,s+1.22\times10^{10})} \quad (2)$$

As Fig. 2 shows, the frequency response of the PZT sensor voltage exhibits a low 3-dB corner frequency at 32 $[Hz]$, as well as a high 3-dB corner frequency at 6 $[kHz]$.

According to Fig. 2, the frequency response of the PZT sensor exhibits a sharp notch at 10.2 $[kHz]$ that does not appear in the laser vibrometer response. As Eq. (2) demonstrates, this notch is quantified by a pair of lightly damped complex zeros with $\omega_n = 6.43\times10^4\ \left[\frac{rad}{s}\right]$, $\zeta = 0.024$, and imposes an upper limit on the bandwidth of the PZT sensor. These complex zeros are the result of the natural frequency of the unloaded Nanopositioner at the same frequency. In Fig. 3, the first mode shape and natural frequency of the unloaded structure is obtained via finite element methods. The value of the natural frequency is 10.8 $[kHz]$ which is very close to the frequency location of the lightly damped complex zeros. As the stage requires negligible external force to vibrate at its unloaded natural frequency, the interaction force between the PZT actuator and the rest of the system is significantly reduced at this frequency. As the PZT sensor responses to the interaction force and since negligible amount of force is transmitted at this frequency, a dominant pair of imaginary zeros are exhibited only in the PZT sensor response but not in the directly measured stage position (by the Laser). As shown in [8], a mass-spring model can also demonstrate the existence of such zero in the interaction force between the PZT actuator and PZT sensor.

Because of the dominant imaginary zero at 10.5 $[kHz]$, the high-3dB corner frequency of the PZT sensor is around 6400 $[Hz]$. Fig. 2 shows that at low frequencies the magnitude response of the PZT sensor reduces by 20 dB per decade as the actuation frequency decreases toward zero. This reduction is accompanied with a phase lead of almost 90 degrees, which indicates the existence of a single zero at the origin. This behavior is in consistency with the response of a resistive load driven by series combination of a voltage source and a capacitor acting as a first-order high-pass filter.

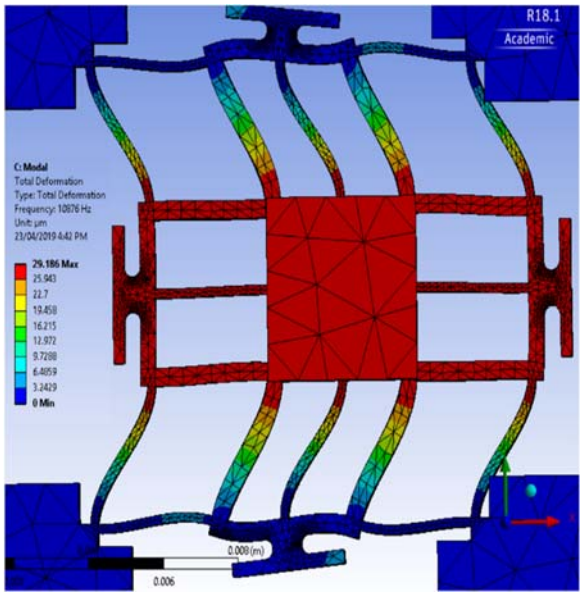

Fig. 3. A finite element modal analysis of the unloaded Nanopositioner predicts the first natural frequency at 10.88 $[kHz]$. The magnified mode shape of the monolithic structure at this frequency indicates the deformation along y-axis [22].

The 3-dB corner frequency of such high-pass filter is

$$\frac{1}{2\pi RC}\ [Hz], \quad (3)$$

where R and C denote the total resistance and capacitance of the filter, respectively. During the frequency response experiment, the PZT sensor is connected to the measurement instruments with the total resistance of $R = 88\ [k\Omega]$. Also, as we measured after preloading, the capacitance of the PZT sensor is around $C = 60\ [nF]$. Therefore, employing (1), the 3-dB corner frequency of the high-pass filter is 30.14 $[Hz]$, which is in close agreement with the measured low corner frequency of 32 $[Hz]$ in Fig. 2. Note that further reduction in the low corner frequency is achievable by connecting the PZT sensor to an instrumentation with a higher resistance. Finally, using the low and high 3-dB corners, the sensor can directly measure the stage displacement in the frequency range of (32-6400) $[Hz]$.

4. Characterization of the PZT Sensor

The calibration process of the PZT sensor on the y-axis is carried out by applying a 500 $[Hz]$ sinusoidal voltage with the range of 0-140 $[V]$, whose frequency is well between the low and the high 3-dB corner frequencies in Fig. 2. The signals from the Laser, the PZT sensor, and the input voltage to the amplifier are simultaneously collected and displayed in Fig. 4(a). In the figure, the voltage value of the PZT sensor and input signal are linearly scaled to have the same extrema as the read out of the laser sensor. Using this experiment, the sensitivity of the PZT sensor is characterized as 1377 $\left[\frac{mV}{\mu m}\right]$. This sensitivity is obtained from the experimentally obtained scale factor as:

$$\text{Senisitivity} = \frac{1}{\text{scale factor}} = \frac{1}{726[\frac{nm}{V}]} \qquad (4)$$

The error value, presented in Fig. 4(b), shows an increase in the amplitude of its vibration around time 1.4 $[ms]$, which is the time when the input signal reaches to its peak value. The inset of Fig. 4(a) shows the close-up view of the signals around this point, where the input signal exhibits a sharp change at peak value. This sharp change is because of the non-smooth profile of sinewave generator, and provokes high frequency vibrations that are close to the resonance mode of the structure. Another similar vibration is also excited when the input reaches its minimum around 0.4 $[ms]$. Further examination of the error value indicates that the frequency of the vibration is around 17 $[kHz]$, which is the fundamental frequency obtained from the frequency response of Fig. 2.

Fig. 5 shows the hysteresis curves obtained by the laser and PZT sensors for the 500 $[Hz]$ sinusoidal actuation voltage with the range of 0-140 $[V]$. It shows that the large hysteretic deviation of the displacement profile, measured by the laser sensor, is precisely captured by the PZT sensor.

In order to validate the scaling factor in Eq. (4), we carry out a similar test for the PZT sensor at a different frequency, whilst the scaling factor is 726 $[\frac{nm}{V}]$. As we can see in Fig. 6, the measurement error at this new frequency is very similar to the measurement error of the 500 $[Hz]$ sinusoidal test, indicating high performance of the PZT chip for displacement measurement within the sensing bandwidth (32-6400) $[Hz]$.

In order to determine accuracy of the PZT sensor, further examination with large amplitude sinusoidal excitation at other frequencies within the sensing bandwidth (32-6400) $[Hz]$ are performed. Fig. 7 and Table 2 report the deviation range and average absolute error of the PZT sensor, respectively. Note that the minor excitation of the resonant mode of the open-loop Nanopositioner at 17 $[kHz]$ due to the non-smooth profile of the input at the peak and the minimum points plays the main role in the error value. As this frequency is far beyond the high-corner frequency, which is 6.4 $[kHz]$, the actual error within the sensing bandwidth is expected to be much smaller.

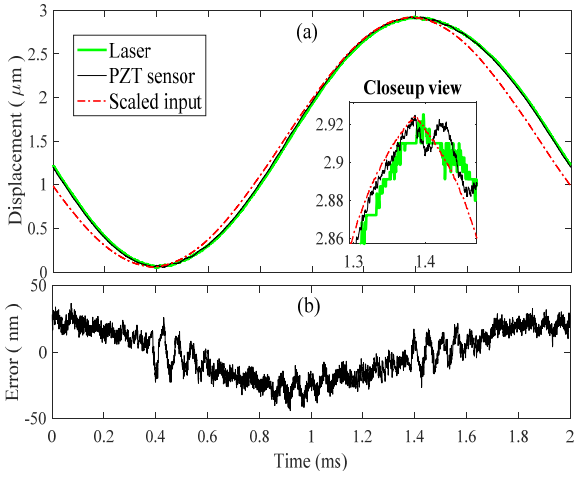

Fig. 4. Calibration test by 500 $[Hz]$ sinusoidal excitation [22].

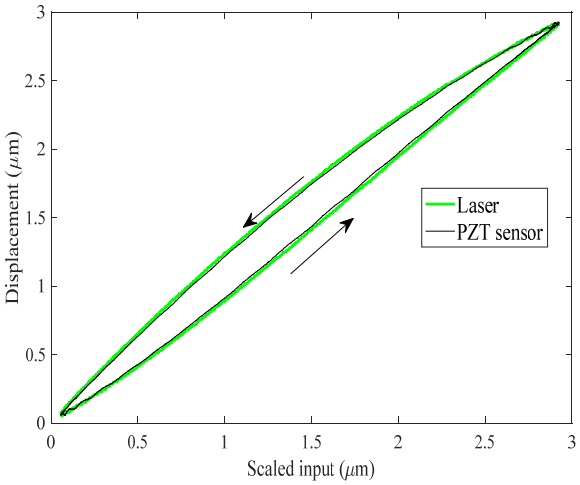

Fig. 5. Hysteresis curves from Laser and PZT sensors [22].

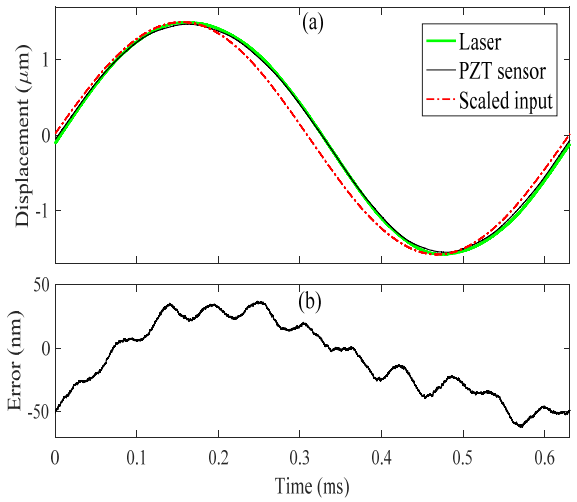

Fig. 6. Validation test at 1583 $[Hz]$ sinusoidal excitation [22].

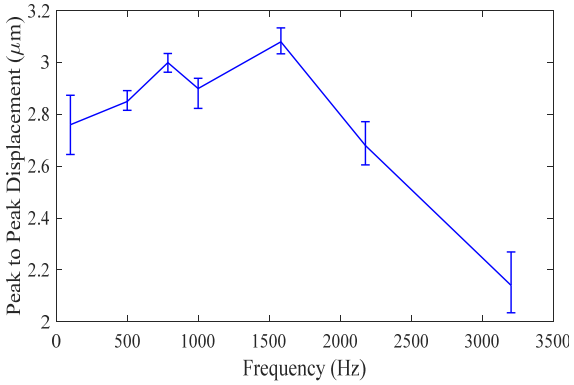

Fig. 7. Evaluation of PZT sensor performance by large signal sinusoidal excitation of y-axis at different frequency values, using a constant calibration coefficient within the sensing bandwidth. The vertical axis represents the peak-to-peak displacement of the stage. The ranges of PZT sensor measurement are indicated by error bars [22].

Table 2. Accuracy of the PZT sensor of y-axis with the constant scaling factor of 726 [nm/V] obtained from the 500 $[Hz]$ calibration test [22].

Freq. (Hz)	100	500	786	1000	1583	2178	3204
RMS Error. (nm)	68.1	17.8	19.3	26.9	25.7	48	70

5. Resolution Study of the PZT Sensor

Generally, the standard deviation of an analog sensor noise is used to quantify the resolution of it [10, 26]. In order to characterize the PZT sensor noise, we tuned the sample rate of our data acquisition device to 50 $[kHz]$ and collected the sensor output without applying any filter while keeping a 70 $[V]$ bias voltage on the PZT actuator. Using the obtained scale factor of 1377 $\left[\frac{mV}{\mu m}\right]$, Fig. 8 displays the time-domain profile, histogram, and spectral density of the PZT sensor noise. The standard deviation of the noise in a 25 $[kHz]$ bandwidth is 0.63 $[nm]$; therefore, the 3σ-resolution of the sensor is 1.9 $[nm]$. The average value for the noise density of the PZT sensor is $\sqrt{A} = 3.5$ $\left[\frac{pm}{\sqrt{Hz}}\right]$. This value can be used to estimate the resolution of the sensor within a desired bandwidth in the range of (f_l, f_h) as described in [18] by

$$3\sigma\text{-resolution} = 3\sqrt{A}\sqrt{f_{nc}\ln\frac{f_h}{f_l} + k_e f_h}, \qquad (5)$$

where f_{nc} is the $1/f$ noise corner frequency, and $k_e \in (1,1.57)$ is a correction factor to consider effect of non-ideal noise filter. For large sensing bandwidth where $f_h \gg f_l$ and $1/f$ noise is negligible, one can assume an ideal noise filter ($k_e = 1$) and Eq. (5) simplifies to $3\sqrt{A}\sqrt{f_h}$.

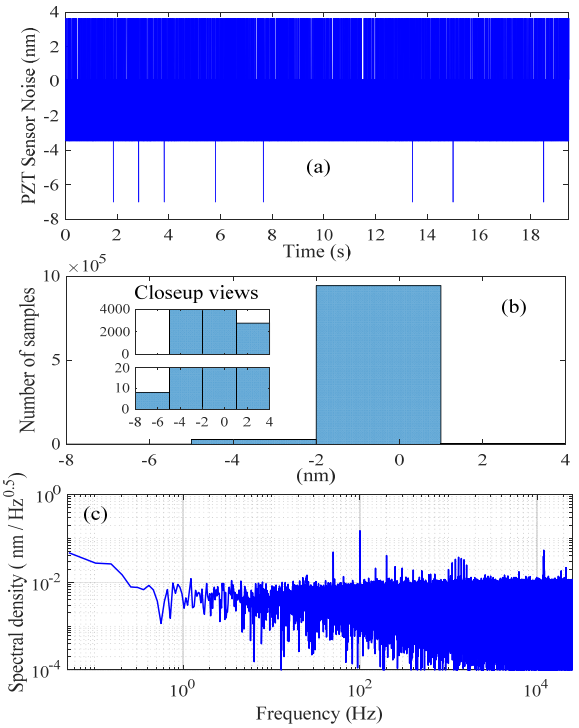

Fig. 8. Noise characteristics of the PZT sensor: (a) noise in time-domain, (b) histogram, and (c) spectral density [22].

6. Application of PZT Sensor in Cross Coupling Displacement Measurement

Cross coupling displacement, or cross talk displacement, is the parasitic displacement of the stage along an unactuated axis due to excitation of the stage along another perpendicular axis. This effect is usually neglected in low speed and short-range nanopositioning systems [27]; however, the effect could become significant if one wants to achieve high-speed scanning rates or large scan area [28]. In atomic force microscopes, for instance, cross coupling can cause distortion in captured images, undesired interactions between cantilever's tip and sample, and even damage to both of them. Therefore, in order to achieve high performance positioning, one may have to measure, and compensate for cross coupling displacement.

To study effectiveness of the proposed PZT sensor in cross coupling displacement measurement, we excited the stage along x-axis whilst the y-axis PZT actuator was open circuited. We applied a large signal sinusoidal excitation (about 140 Vpp) to the PZT actuator of x-axis and measured the displacement of the stage along y-axis by the laser interferometer and the PZT sensor output of y-axis. The results are shown in Fig. 9 after scaling the sensor signals by positive constants reported in the figure legends, to have almost the same peak-to-peak value as the y-axis displacement measured by the laser sensor. This observation shows that the y-axis PZT sensor can also provide acceptable displacement of the stage along y-axis even when we drive the stage

along x-axis only. However, the scale factor of y-axis PZT sensor for cross-coupling displacement measurement is different from the scale factor obtained during the normal operation in Section 4, where the stage is driven along y-axis only.

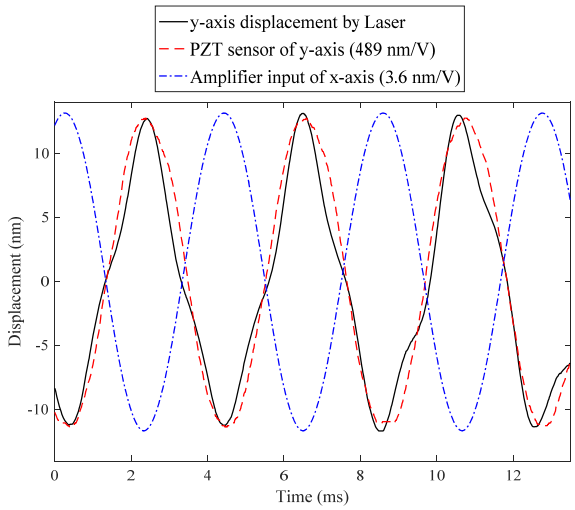

Fig. 9. Response of PZT sensor of y-axis and stage displacement along y-axis, while the y-axis actuator is open circuited and the x-axis one is driven by a large signal 240 $[Hz]$ sinusoidal excitation. The scaling factor of the PZT sensor for the cross coupling motion is 489 $\left[\frac{nm}{V}\right]$.

The foregoing cross coupling measurement indicates a peak-to-peak value of 24 $[nm]$ along y-axis during large signal excitation of x-axis. During this large signal excitation, the stage is displaced in a range of 3.074 $[\mu m]$ along x-axis, as indicated by the data depicted in Fig. 10. Hence, the amount of cross-coupling from x-axis to y-axis is about

$$\frac{0.024}{3.074} = 7.81 \times 10^{-3} = -42\ dB$$

As the value of the cross coupling is very small, the interactions in force and displacement between x and y axes are insignificant. As a result, the PZT displacement sensors are notable candidates for nanopositioners in which the cross coupling is small. Considering that most of the nanopositioners are designed to meet very small cross coupling, the proposed PZT sensor is applicable to most piezo-driven nanopositioners.

7. Conclusions

We showed in this study that the time-varying displacement of nanopositioning stages can be measured in a real-time fashion by piezoelectric ceramics. The PZT sensors have a lightly damped minimum-phase zero at the fundamental frequency of the unloaded monolithic nanopositioner. The pair of zeros do not appear in the response of the laser sensor for stage displacement and, therefore, impose a limitation on the high corner frequency of the PZT sensor. Nevertheless, considering the advantages of the proposed sensor, including small foot-print, low cost, small noise level, compactness, and no requirement to hefty instruments for signal conditioning, PZT sensors can be regarded as ideal displacement sensors for small-size and low-cost applications where the displacement exhibits a time-varying behavior.

Acknowledgement

This work has been partially sponsored by the project PolyREM (Emergence Sorbonne Université), the French government research program Investissements d'avenir through the Robotex Equipment of Excellence (ANR-10-EQPX-44), the University of Newcastle Australia, and the National Natural Science Foundation of China under grant Number 51729501. We would like to thank Dr. Yuen K. Yong and Prof. Andrew J. Fleming for their valuable advices.

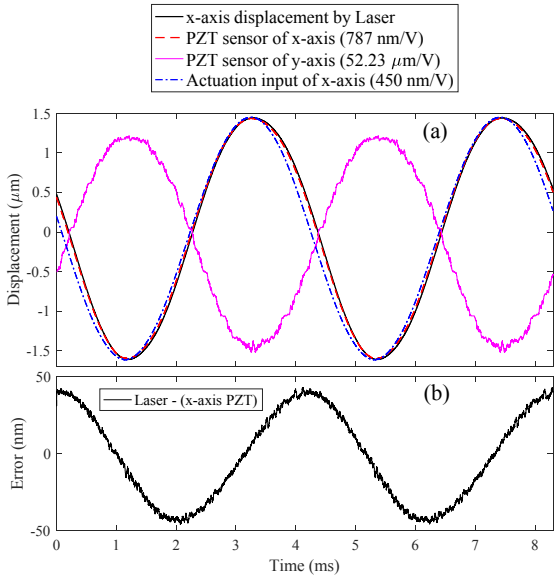

Fig. 10. (a) Responses of the PZT sensors of x and y axes and stage displacement along x-axis during large signal excitation of x-axis actuator by a 240 $[Hz]$ sinusoid, while the y-axis actuator is open circuited. (b) Error of x-axis PZT sensor in measurement of x-axis displacement with a scale factor of 0.787$[\frac{\mu m}{V}]$.

References

[1]. S. S. Aphale, A. J. Fleming, S. O. R. Moheimani, High speed nano-scale positioning using a piezoelectric tube actuator with active shunt control, *IET Micro & Nano Letters*, Vol. 2, Issue 1, 2007, pp. 9–12.

[2]. S. Polit, J. Dong, Development of a high-bandwidth XY nanopositioning stage for high-rate Micro-

/Nanomanufacturing, *IEEE/ASME Transactions on Mechatronics*, Vol. 16, Issue 4, Aug 2011, pp. 724–733.

[3]. C.-X. Li, G.-Y. Gu, M.-J. Yang, L.-M. Zhu, Design, analysis and testing of a parallel-kinematic high-bandwidth XY nanopositioning stage, *Review of Scientific Instruments*, Vol. 84, Issue 12, 2013, p. 125111.

[4]. A. San-Millan, V. Feliu-Batlle, S. S. Aphale, Application of a fractional order integral resonant control to increase the achievable bandwidth of a nanopositioner, in *Proceedings of the 20th IFAC World Congress*, Vol. 50, 2017, pp. 14539–14544.

[5]. M. Altaher, S. S. Aphale, High-precision control of a piezodriven nanopositioner using fuzzy logic controllers, *Computers*, Vol. 7, Issue 1, 2018, pp. 1-17.

[6]. H. Huang, H. Zhao, Z. Yang, Z. Fan, S. Wan, C. Shi, Z. Ma, Design and analysis of a compact precision positioning platform integrating strain gauges and the piezoactuator, *Sensors*, Vol. 12, Issue 7, July 2012, pp. 9697–9710.

[7]. E. Guliyev, B. E. Volland, Y. Sarov, T. Ivanov, M. Klukowski, E. Manske, I. W. Rangelow, Quasi-monolithic integration of silicon-MEMS with piezoelectric actuators for high-speed non-contact atomic force microscopy, *Measurement Science and Technology*, Vol. 23, Issue 7, 2012, p. 074012.

[8]. A. J. Fleming, K. K. Leang, Integrated strain and force feedback for high performance control of piezoelectric actuators, *Sensors and Actuators A: Physical*, Vol. 161, Issue 1-2, 2010, pp. 256–265.

[9]. Y. K. Yong, A. J. Fleming, High-speed vertical positioning stage with integrated dual-sensor arrangement, *Sensors and Actuators A: Physical*, Vol. 248, Sep. 2016, pp. 184–192.

[10]. C. Lee, S. M. Salapaka, Robust broadband nanopositioning: fundamental trade-offs, analysis, and design in a two degree-of-freedom control framework, *Nanotechnology*, Vol. 20, Issue 3, 2009, p. 035501.

[11]. Y. K. Yong, S. O. R. Moheimani, B. J. Kenton, K. K. Leang, Invited review article: High-speed flexure-guided nanopositioning: Mechanical design and control issues, *Review of Scientific Instruments*, Vol. 83, Dec. 2012, p. 121101.

[12]. K. H. Koh, T. Kobayashi, J. Xie, A. Yu, C. Lee, Novel piezoelectric actuation mechanism for a gimbal-less mirror in 2D raster scanning applications, *Journal of Micromechanics and Microengineering*, Vol. 21, June 2011, p. 075001.

[13]. T. Aimono, Optical deflector including piezoelectric sensor incorporated into outermost piezoelectric cantilever, US Patent 13/846,028, Nov. 2013.

[14]. Y. Park, S. Moon, J. Lee, K. Kim, S.-J. Lee, J.-H. Lee, Gimbal-less two-axis electromagnetic microscanner with twist mechanism, *Micromachines*, Vol. 9, Issue 5, May 2018, p. 219.

[15]. K. An, S. Hong, S. Han, H. Lee, J. Yeo, S. H. Ko, Selective sintering of metal nanoparticle ink for maskless fabrication of an electrode micropattern using a spatially modulated laser beam by a digital micromirror device, *ACS Applied Materials & Interfaces*, Vol. 6, Issue 4, Feb. 2014, pp. 2786–2790. PMID: 24471931.

[16]. K. Bakshi, A. V. Mulay, A review on selective laser sintering: A rapid prototyping technology, *IOSR Journal of Mechanical and Civil Engineering,* in *Proceedings of the 5th National Conference on Recent Developments in Mechanical Engineering (RDME-2016)*, Vol. 04, Mar. 2016, pp. 53–57.

[17]. W. Ameen, A. M. Ghaleb, M. Alatefi, H. Alkhalefah, A. Alahmari, An overview of selective laser sintering and melting research using bibliometric indicators, *Virtual and Physical Prototyping*, Vol. 13, Issue 4, July 2018, pp. 282–291/

[18]. A. J. Fleming, A review of nanometer resolution position sensors: operation and performance, *Sensors and Actuators A: Physical*, Vol. 190, Feb. 2013, pp. 106–126.

[19]. G. Gautschi, Piezoelectric Sensorics: force, strain, pressure, acceleration and acoustic emission sensors, materials and amplifiers, *Springer-Verlag*, 2002.

[20]. J. Tichý, *et al*., Fundamentals of Piezoelectric Sensorics: mechanical, dielectric, and thermodynamics properties of piezoelectric materials, *Springer-Verlag*, 2010.

[21]. M. Umapathy, Piezoelectric based resonance displacement sensor, in *Proceedings of the IEEE Sensors Applications Symposium*, Galveston, TX, USA, 2013, pp. 193–196.

[22]. A. Bazaei, M. Boudaoud, M. Hemmasian Ettefagh, Z. Chen, S. Régnier, Displacement Sensing by Piezoelectric Transducers in High-Speed Lateral Nanopositioning, *IEEE Sensors Journal,* Vol. 19, Issue 20, 2019, pp. 9156-9165.

[23]. A. Bazaei, M. Boudaoud, M. Hemmasian Ettefagh, Z. Chen, S. Régnier, Direct Sensing of Time-Varying Displacement in Nanopositioners by Piezoelectric Ceramics Transducers, in *Proceedings of the 5th International Conference on Sensors and Electronic Instrumentation Advances (SEIA'2019*), Tenerife, (Canary Islands), Spain, 25-27 September 2019, pp. 161-165.

[24]. M. Boudaoud, Y. Le Gorrec, Y. Haddab, P. Lutz, Gain scheduling control of a nonlinear electrostatic microgripper: design by an eigenstructure assignment with an observer based structure, *IEEE Transactions on Control Systems Technology*, Vol. 23, Issue 4, 2015, pp. 1255-1267.

[25]. Adriaens H. J. M. T. S., Willem L. De Koning, Reinder Banning, Modeling piezoelectric actuators, *IEEE/ASME Transactions on Mechatronics*, Vol. 5, Issue 4, 2000, pp. 331-341.

[26]. I. Cemer, S. Miller, K. Foust, Noise Measurement, *FierceEectronics*, 1 Feb. 2011, https://www.fierceelectronics.com/embedded/noise-measurement

[27]. El Rifai Osamah M., Kamal Youcef-Toumi, Coupling in piezoelectric tube scanners used in scanning probe microscopes, in *Proceedings of the IEEE American Control Conference*, Vol. 4, 2001.

[28]. Wu Ying, *et al*., A control approach to cross-coupling compensation of piezotube scanners in tapping-mode atomic force microscope imaging, *Review of Scientific Instruments,* Vol. 80, Issue 4, 2009, 043709.

Published by International Frequency Sensor Association (IFSA) Publishing, S. L., 2019 (http://www.sensorsportal.com).